 doi:10.20944/preprints202205.0200.v1

Article

The Membrane Potential has a Primary Key Equation

Hirohisa Tamagawa [1,†,*], Toi Nakahata [1,†], Ren Sugimori [1,†] and Bernard Delalande [2,†]

[1] Department of Mechanical Engineering, Faculty of Engineering, Gifu University, 1-1 Yanagido, Gifu, Gifu, 501-1193 Japan; tmgwhrhs@gifu-u.ac.jp, y3031086@edu.gifu-u.ac.jp; eyemask2000@gmail.com
[2] 280 avenue de la Pierre Dourdant, 38290 La Verpilliere, France; bernard@somasimple.com
* Correspondence: tmgwhrhs@gifu-u.ac.jp; Tel.:+81-58-293-2529 (H.T.)
† These authors contributed equally to this work.

Abstract: Although there is a common physiological notion that the origin of the membrane potential is attributed to transmembrane ion transport, it is theoretically possible to explain its generation by the mechanism of ion adsorption. It was previously suggested that the ion adsorption mechanism led even to the potential formulas which are even identical to either the famous Nernst equation or Goldman-Hodgkin-Katz equation. Our further analysis shown in this paper indicates that the potential formula based on the ion adsorption mechanism leads to one equation which is the function of material surface charge density and the material surface potential. Furthermore, we confirmed that the equation holds in all the different experimental systems we studied. Although we have not succeeded in elucidating why such an equation is established, the equation appears to be the key equation governing the characteristics of the membrane potential regardless of the systems in question.

Keywords: membrane potential; Nernst equation; ion adsorption; surface charge; surface potential

1. Introduction

The authors studied the mechanism of membrane potential generation from the perspective of the ion adsorption mechanism [1–3]. Previously, Tamagawa and Ikeda derived a membrane potential formula based on ion adsorption, which is identical to the Goldman-Hodgkin-Katz equation (GHK eq.) [4,5]. However, the basis of the derived formula has nothing to do with the transmembrane ion transport on which the GHK eq. is based. When further investigating the mechanism of generation of the membrane potential based on ion adsorption, we noticed that the membrane potential seems to obey an equation which is the function of the material surface charge density and its surface potential. Thus, we would like to discuss this equation experimentally and theoretically in this paper.

Before presenting the authors' work, the notations used in common throughout this work are given in Table 1.

Table 1. Notations used throughout this work

ϵ	relative permittivity of water	80	
ϵ_0	vacuum permittivity	8.85×10^{-12}	$/\ Fm^{-1}$
e	elementary charge	1.60×10^{-19}	$/\ C$
k	Boltzmann constant	1.38×10^{-23}	$/\ m^2kgs^{-2}$
T	temperature	298	$/\ K$
z_i	valency of ion i		
β	$\beta \equiv e/2kT$		

2. Background

The surface potential of $AgCl$-coated Ag plate (hereafter called $AgCl$ plate) immersed in a single KCl solution system, which is illustrated in Fig. 1, exhibits the nonzero potential.

Preprints (www.preprints.org) | NOT PEER-REVIEWED | Posted: 16 May 2022 doi:10.20944/preprints202205.0200.v1

It varies by the KCl concentration as shown in Fig. 2. It is possible to reproduce this potential profile by the GHK eq. But Tamagawa and Ikeda derived an alternative formula to the GHK eq. by assuming that the spatial fixation of mobile ions by the adsorption on the surface of the $AgCl$ plate generates the membrane potential [5].

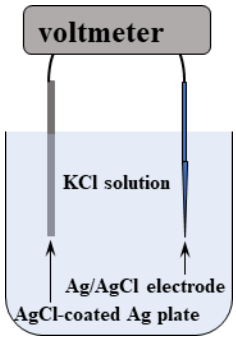

Figure 1. Single KCl solution system for measuring the $AgCl$ plate surface potential

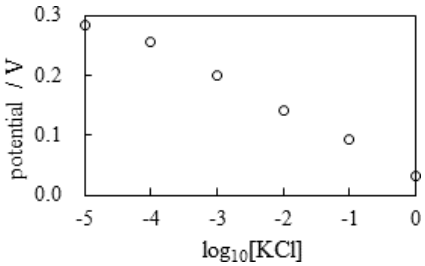

Figure 2. Experimentally measured $AgCl$ plate surface potential in a single KCl solution system vs. $\log_{10}[KCl]$ (Data from the ref. [5] Although the $AgCl$ used in the ref. [5] was $AgCl$-wire instead of $AgCl$-plate, the potential is independent of the $AgCl$ morphology.

First, the authors will review the Tamagawa and Ikeda's work [5]. Assuming that Cl^- ions are adsorbed on the surface of the $AgCl$ plate [6], the authors attempt to derive a potential formula for the experimental system of Fig. 1 as below (see notation table, Table 2) [5].

Table 2. Notations used in the section 2. **Background**

Q_i^S	bulk phase concentration of i in the single KCl solution ($i = K^+, Cl^-$)
Q_i^k	bulk phase concentration of i in the k phase of two KCl-solution system, ($k = L(eft), R(ight)$)
s	surface adsorption site for the mobile anion Cl^-
$[s]_T$	total ion adsorption site density of the $AgCl$ plate
K_{Cl}	binding constant between Cl^- and s, $K_{Cl} \equiv [sCl]/[s][Cl]\|_{x=0}$
ϕ_0^S	$AgCl$ surface potential of a single KCl-solution system
ϕ^S	KCl solution potential of the single KCl-solution system
ϕ_0^k	$AgCl$ surface potential in k phase of two KCl-solution system
ϕ^k	KCl solution potential in k phase of two KCl-solution system
$\Delta\phi$	potential across the $AgCl$ plate
$\sigma\|_{x=0}$	$AgCl$ plate surface charge density
σ_0	$AgCl$ plate surface charge density with no ion adsorption

Inserting the coordinate system as shown in Fig. 3, the ionic concentration at x is given by Eq. 1.

Preprints (www.preprints.org) | NOT PEER-REVIEWED | Posted: 16 May 2022 doi:10.20944/preprints202205.0200.v1

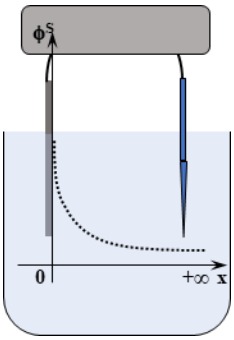

Figure 3. Experimental setup for measuring the surface potential of the $AgCl$ plate. The dotted curve represents the expected potential profile.

$$[i](x) = [i]_{x=+\infty} \exp(-z_i \beta \phi_0^S) = Q_i^S \exp(-z_i \beta \phi^S) \tag{1}$$

The surface charge density of the $AgCl$ plate is given by Eq. 2.

$$\sigma|_{x=0} = 2\sqrt{\epsilon\epsilon_0 Q_{Cl}^S kT} \sinh(\beta\phi_0^S) \tag{2}$$

The $AgCl$ plate exhibits the non-zero positive surface potential, 0.309 V, even in deionized water (0M KCl solution). Therefore, the $AgCl$ plate is assumed to carry the hypothetical positive charges originally in an aqueous solution. Denoting the original surface charge density by σ_0, the surface charge density of the $AgCl$ plate when the adsorption of Cl^- takes place is given by Eq. 3.

$$\sigma|_{x=0} = \sigma_0 - e[s]_T \frac{K_{Cl} Q_{Cl}^S \cdot exp(2\beta\phi_0^S)}{1 + K_{Cl} Q_{Cl}^S \cdot exp(2\beta\phi_0^S)} \tag{3}$$

Eq.2 can be arranged into Eq. 4.

$$\sigma|_{x=0} \sim \sqrt{Q_{Cl}^S} \sinh(\beta\phi_0^S) \tag{4}$$

Substituting the experimental condition Q_{Cl}^S and the experimentally measured potential ϕ_0^S into the RHS of Eq. 2, the quasi-constant results summarized in Table 3 was obtained. The data deviate from the constant at the lowest and highest concentration limits. The theoretical computational curves of RHS of Eq. 4 for the individual Q_{Cl}^S are shown in Fig. 4 and the corresponding data of the RHS of Eq. 4 shown in Table 3 is also demonstrated in Fig. 4 by the symbol "•".

Table 3. Experimental Q_{Cl}^S and ϕ_0^S and Computational data of $\sqrt{Q_{Cl}^S}\sinh(\beta\phi_0^S)$

Q_{Cl}^S / M	0	10^{-5}	10^{-4}	10^{-3}	10^{-2}	10^{-1}	10^{0}
ϕ_0^S / V	0.309	0.284	0.257	0.201	0.141	0.092	0.032
$\sqrt{Q_{Cl}^S}\sinh(\beta\phi_0^S)^\dagger$	-	0.459	0.845	0.881	0.836	0.970	0.684

† $\sqrt{Q_{Cl}^S}\sinh(\beta\phi_0^S)$ is almost constant, it deviates from the constant only at the lowest and the highest concentration limits.

Preprints (www.preprints.org) | NOT PEER-REVIEWED | Posted: 16 May 2022 doi:10.20944/preprints202205.0200.v1

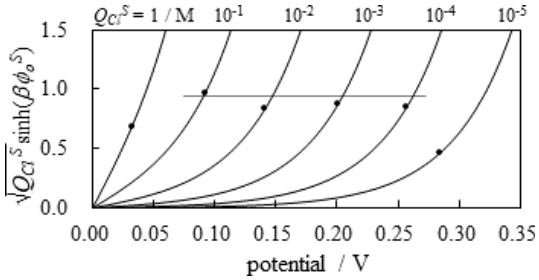

Figure 4. The theoretical computational curves of RHS of Eq. 4 are shown. The corresponding data shown in Table 2 is also shown by the symbol "•." The dashed line represents "RHS of Eq. 4 = const."

Since Eq. 2 can be considered approximately as a constant, Eq. 4 is also a constant (The meaning of Eq. 4 will be later discussed.). Since Eq. 2 is constant, Eq. 3 is constant. Since σ_0, e and $[s]_T$ are constant, Eq. 5 is derived. Solving Eq. 5 with respect to ϕ_0^S gives Fig. 6.

$$K_{Cl}Q_{Cl}^S \cdot exp(2\beta\phi_0^S) \sim A, \quad A \text{ is introduced here as a constant.} \tag{5}$$

$$\phi_0^S \sim \frac{kT}{e} \ln \frac{A}{K_{Cl}Q_{Cl}^S} \tag{6}$$

The authors carried out a measurement of the potential between two KCl solutions separated by the $AgCl$ plate. Figure 5 shows the experimental setup. The potential generated across the $AgCl$ plate separating two KCl solutions was measured by changing the concentration of the Left phase KCl solution from 10^{-5}M to 1M while the concentration of the Right phase KCl was maintained at 10^{-4}M where the potential of the Right phase KCl solution was defined as the 0V reference. The potential measurements were carried out while changing the concentration of the KCl solution from 10^{-5}M to 1M. Then again, the same potential measurement was performed while replacing the Right 10^{-4}M KCl solution with a 10^{-2}M KCl solution. The measured results are all summarized in Table 4.

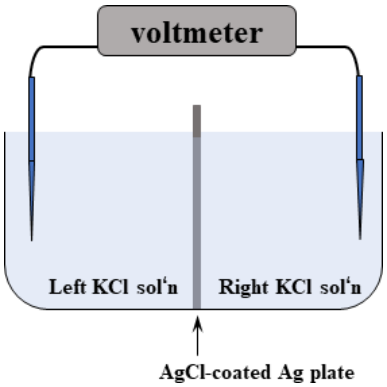

Figure 5. Experimental setup for measuring the potential across the two KCl solutions

The experimental setup can be considered as a system consisting of two independent single KCl solution systems, the Left and Right phase, as shown in Fig. 6 with their own coordinate systems (x^k, ϕ^k) $(k = L, R)$.

As clearly shown in Fig. 6, the potential across the $AgCl$ plate, $\Delta\phi$, is represented by the difference between "the negative valued of the surface potential of the Left phase" and the "that of the Right phase", and it is most clearly represented by Eq. 7.

Preprints (www.preprints.org) | NOT PEER-REVIEWED | Posted: 16 May 2022 doi:10.20944/preprints202205.0200.v1

Table 4. Experimentally measured potentials across the *AgCl* plate separating two *KCl* solutions.

[KCl]† / M	10^{-5}	10^{-4}	10^{-3}	10^{-2}	10^{-1}	1
$\Delta\phi$ / V			$[KCl]_R^{\ddagger} = 10^{-4}$M			
	-0.024	0.000	0.053	0.112	0.161	0.220
$\Delta\phi$ / V			$[KCl]_R^{\ddagger} = 10^{-2}$M			
	-0.125	-0.102	-0.053	0.000	0.053	0.103

† Left phase *KCl* concentration
‡ Right phase *KCl* concentration

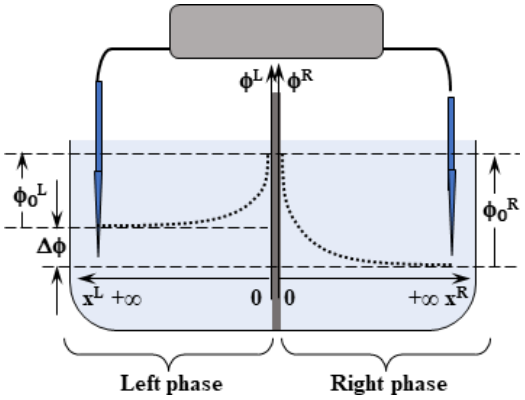

Figure 6. Two independent single KCl solution systems shown in Fig. 5. These two systems carry their individual coordinate systems. The dotted curves represent the expected potential profiles.

$$\Delta\phi = (-\phi_0^L) - (-\phi_0^R) \tag{7}$$

Left phase" and "Right phase" of the experimental setup in Fig. 6 are equivalent to the system illustrated in Fig. 3. Therefore, ϕ_0^k (k = L(eft), R(ight)) could be given by Eq. 8. Namely, ϕ_0^k of Eq. 8 is equivalent to Eq. 6.

$$\phi_0^k \sim \frac{kT}{e} \ln \frac{A}{K_{Cl} Q_{Cl}^k} \quad Q_{Cl}^k : \text{bulk phase } [Cl^-] \text{ in } k \text{ phase.} \tag{8}$$

Therefore, $\Delta\phi$ is given by the Eq. 9, and it is identical to the well-known Nernst equation (Nernst eq.) [7]. Thus, the Nernst eq. in the physiological sense can be derived on the basis that the potential is generated by the spatial binding of ions (the ion adsorption onto the surface of the *AgCl* plate), whereas the existing idea is that the Nernst eq. is derived on the basis that the potential is generated by the transmembrane transport (across the plasma membrane) of ions [1–3].

$$\Delta\phi = \left(-\frac{kT}{e} \ln \frac{A}{K_{Cl} Q_{Cl}^L} \right) - \left(-\frac{kT}{e} \ln \frac{A}{K_{Cl} Q_{Cl}^R} \right) = -\frac{kT}{e} \ln \frac{Q_{Cl}^R}{Q_{Cl}^L} \tag{9}$$

$\Delta\phi$ of Eq. 9 can be directly measured experimentally, and these experimental data is shown in Table 3. Eq. 9 begins with Eq. 7. On the other hand, ϕ_0^k of Eq. 7 virtually corresponds to ϕ_0^S shown in Table 3. The authors attempt to reproduce $\Delta\phi$ in Table 4 by applying the experimental surface potential data of Table 3 into the RHS of Eq. 7. Figure 7 shows the results, and the ion adsorption mechanism-based computed potential

Preprints (www.preprints.org) | NOT PEER-REVIEWED | Posted: 16 May 2022 doi:10.20944/preprints202205.0200.v1

represented by the symbol "•" quite precisely reproduces the experimentally measured potential represented by the symbol "◯".

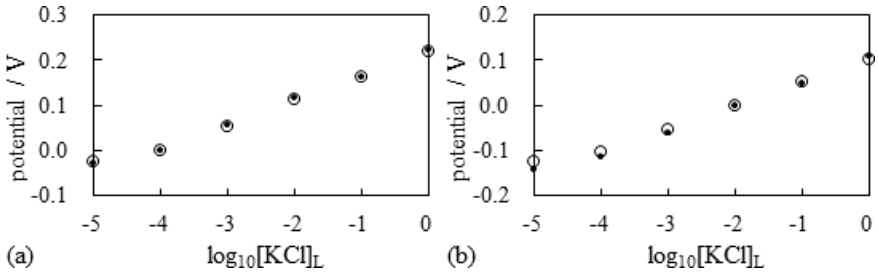

Figure 7. Potential across the $AgCl$ plate intervening two KCl solutions (a) when $[KCl]_R = 10^{-4}$M (b) when $[KCl]_R = 10^{-2}$M ◯: Experimentally measured $\Delta\phi$ shown in Table 4, •: $\Delta\phi$ computed by applying the experimental data shown in Table 3 into the RHS of Eq. 7

Thus, no transmembrane ion transport is required to generate the non-zero potential across the $AgCl$ plate that separates two KCl solutions. The potential formula based on ion adsorption Eq. 9 is identical to the Nernst eq. Therefore, it is natural to raise a question: Isn't the membrane potential generated across the actual plasma membrane due to spatial binding of mobile ions rather than transmembrane ion transport?

3. Potential generation based on ion adsorption

What is described in the previous section is the summary of the work of Tamagawa and Ikeda and a more in-depth analysis of the work [5]. In this work, the authors investigated whether their work is applicable to other electrolyte solution systems. The authors performed measurements of the potential generated through (i) a lithium glass, (ii) an anionic hydrogel and (iii) a cationic hydrogel.

3.1. Potential across lithium glass

First, the notation table Table 5 is introduced for the analysis described in this section. Using the same experimental setup illustrated in Fig. 5, the potential generated across the lithium glass (LICGC^{TM}PW-01, OHARA INC., Kanagawa, Japan) between two $LiCl$ solutions was measured and the $LiCl$ concentration and measured potentials are summarized in Table 6 with the ion concentration conditions. Then the theoretical treatment described in the previous section is performed (Please refer to the notation table Table 5). Although the data sheet for lithium glass states that lithium glass is permeable to Li^+, the authors hypothesized that lithium glass could adsorb Li^+ only at its surface adsorption site. Therefore, by designating the lithium glass adsorption site as "s", the mass action law says Eq. 10, and it turns out to be Eq. 11 where K_{Li} is the association constant.

Table 5. Notations used in the section 3.1

K_{Li}	binding constant between Li^+ and s, $K_{Li} \equiv [sLi^+]/[s][Li^+]\|_{x=0}$
$\Delta\phi$	experimental potential across the lithium glass
$\Delta\Phi$	potential across the lithium glass defined by $(-\phi_0^L)$ - $(-\phi_0^R)$
$[i]_J$	concentration of i in J phase, $J = L(eft), R(ight)$
$Q^J_{i+\infty}$ $(\equiv Q^J_{+\infty})$	bulk phase concentration of i in J phase
ρ^J	charge density in the J phase
ϕ_0^J	lithium glass surface potential in J phase
ϕ^J	$LiCl$ solution potential in J phase
$\sigma^J\|_{x=0}$	lithium glass surface charge density in J phase
s	surface adsorption site for Li^+ on the lithium glass surface
$[s]^T_J$ $(\equiv [s]_T)$	total ion adsorption site density of the lithium glass surface in J phase

Preprints (www.preprints.org) | NOT PEER-REVIEWED | Posted: 16 May 2022 doi:10.20944/preprints202205.0200.v1

Table 6. Experimental conditions and potential through the lithium glass plate separating two *LiCl* solutions

$[LiCl]_L^{\dagger}$ / M	10^{-5}	10^{-4}	10^{-3}	10^{-2}	10^{-1}	1
$\Delta\phi$ / V			$[LiCl]_R^{\ddagger} = 10^{-5}$M			
	-0.002	-0.023	-0.079	-0.133	-0.192	-0.263
$\Delta\phi$ / V			$[LiCl]_R^{\ddagger} = 10^{-4}$M			
	0.027	0.007	-0.048	-0.102	-0.163	-0.231
$\Delta\phi$ / V			$[LiCl]_R^{\ddagger} = 10^{-3}$M			
	0.084	0.052	0.001	-0.058	-0.115	-0.172
$\Delta\phi$ / V			$[LiCl]_R^{\ddagger} = 10^{-2}$M			
	0.131	0.105	0.054	-0.006	-0.054	-0.114
$\Delta\phi$ / V			$[LiCl]_R^{\ddagger} = 10^{-1}$M			
	0.202	0.170	0.115	0.058	0.000	-0.060
$\Delta\phi$ / V			$[LiCl]_R^{\ddagger} = 1$M			
	0.258	0.225	0.168	0.112	0.055	0.000

† Left phase *LiCl* concentration
‡ Right phase *LiCl* concentration

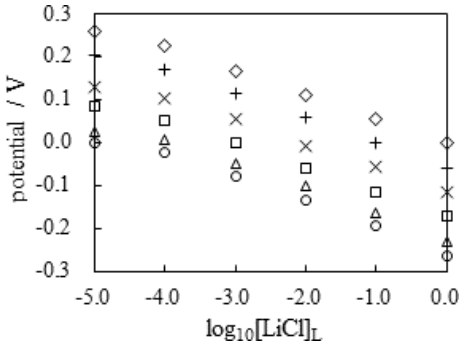

Figure 8. Potential across the lithium glass separating two *LiCl* solutions vs. $[LiCl]_L$ $[LiCl]_R$ (◇: 10^{-5}M +: 10^{-4}M ×: 10^{-3}M □: 10^{-2}M △: 10^{-1}M ◯: 1M)

$$Li^+ + s <=> sLi^+ \tag{10}$$

$$K_{Li} = \frac{[sLi^+]_J}{[s]_J [Li^+]_J|_{x=0}}, \quad J = L(\text{eft}), R(\text{ight}) \tag{11}$$

The system to be theoretically treated is same as the system illustrated in Fig. 6 in case where both Left and Right phases are the *LiCl* solutions instead of *KCl* solutions. Eq. 12 represents the ion Boltzmann distribution.

$$[i]_J = Q^J_{i+\infty} \exp(-z_i \beta \phi^J_0), \quad i = Li^+, Cl^- \tag{12}$$

Solving the Poisson-Boltzmann equation (P.B. eq.) given by Eq. 13 under the conditions represented by Eqs. 14 ∼ 17, we obtain $d\phi^J/dx^J$ represented by Eq. 18, where Eq. 15 is given due to electroneutrality.

Preprints (www.preprints.org) | NOT PEER-REVIEWED | Posted: 16 May 2022 doi:10.20944/preprints202205.0200.v1

$$\frac{d^2\phi^J}{dx^{J2}} = -\frac{\rho^J}{\epsilon\epsilon_o} = -\frac{e}{\epsilon\epsilon_o}[Q^J_{Li+\infty}\exp(-2\beta\phi^J) - Q^J_{Cl+\infty}\exp(+2\beta\phi^J)] \tag{13}$$

$$\rho^J = eQ^J_{+\infty}[\exp(-2\beta\phi^J) - \exp(+2\beta\phi^J)] \tag{14}$$

$$\text{where } Q^J_{+\infty} \equiv Q^J_{Li+\infty} = Q^J_{Cl+\infty} \tag{15}$$

$$\phi^J \to 0 \ \ (x^J \to +\infty) \tag{16}$$

$$\frac{d\phi^J}{dx^J} \to 0 \ \ (x^J \to +\infty) \tag{17}$$

$$\frac{d\phi^J}{dx^J} = -2\sqrt{\frac{2Q^J_{+\infty}kT}{\epsilon\epsilon_0}}\sinh(\beta\phi^J) \tag{18}$$

Eq. 19 holds due to electroneutrality where $\sigma^J|_{x=0}$ represents the surface charge density of lithium glass.

$$\sigma^J|_{x=0} + \int_0^{+\infty}\rho^J dx \tag{19}$$

The use of Eqs. 18 and 19 leads to Eq. 20.

$$\sigma^J|_{x=0} = 2\sqrt{2\epsilon\epsilon_o Q^J_{+\infty}kT}\sinh(\beta\phi^J_0) \tag{20}$$

The total adsorption site density $[s]^J_T$ on the lithium glass surface is given by Eq. 21. Eq. 22 corresponds to the well-known Langmuir isotherm [7].

$$[s]^T_J = [s]_J + [sLi^+]_J \tag{21}$$

Eq. 22 is derived using Eqs 11 and 21.

$$[sLi^+]_J = \frac{K_{Li}[s]^T_J[Li^+]_J|_{x=0}}{1 + K_{Li}[Li^+]_J|_{x=0}} \tag{22}$$

Eq. 22 can be further arranged into Eq. 23 using Eq. 12 where $[s]_T$ is defined by Eq. 24. Then, the LHS of Eq. 20 can be given by Eq. 25 as well.

$$[sLi^+]_J = \frac{K_{Li}[s]^T_J Q^J_{+\infty}\exp(-2\beta\phi^J_0)}{1 + K_{Li}Q^J_{+\infty}\exp(-2\beta\phi^J_0)} \tag{23}$$

$$[s]_T \equiv [s]^T_J \tag{24}$$

Preprints (www.preprints.org) | NOT PEER-REVIEWED | Posted: 16 May 2022 doi:10.20944/preprints202205.0200.v1

$$\sigma^J|_{x=0} = e[sLi^+]_J = e\frac{K_{Li}[s]_T Q^J_{+\infty}\exp(-2\beta\phi^J_0)}{1+K_{Li}Q^J_{+\infty}\exp(-2\beta\phi^J_0)} \tag{25}$$

Since Eq. 20 is same as Eq. 25, Eq. 26 is derived.

$$\frac{\sigma^J|_{x=0}}{Q^J_{+\infty}} = \frac{eK_{Li}[s]_T\exp(-2\beta\phi^J_0)}{1+K_{Li}Q^J_{+\infty}\exp(-2\beta\phi^J_0)} = 2\sqrt{\frac{2\epsilon\epsilon_o kT}{Q^J_{+\infty}}}\sinh(\beta\phi^J_0) \tag{26}$$

Now, let us assume that the rightmost term of Eq. 26 is constant thus it means Eq. 27. Furthermore, if ϕ^J_0 is high enough such that Eq. 28 is sufficed Ⓐ, Eq. 27 can be approximated by Eq. 29 Ⓑ.

$$\frac{1}{\sqrt{Q^J_{+\infty}}}\sinh(\beta\phi^J_0) \sim const. \tag{27}$$

$$\sinh(\beta\phi^J_0) \sim \exp(\beta\phi^J_0) \tag{28}$$

$$\frac{1}{\sqrt{Q^J_{+\infty}}}\sinh(\beta\phi^J_0) \sim \frac{1}{\sqrt{Q^J_{+\infty}}}\exp(\beta\phi^J_0) = B \tag{29}$$

B is introduced here as a constant.

Solving Eq. 29 with respect to ϕ^J_0, Eq. 30 is derived.

$$\phi^J_0 \sim \frac{kT}{e}\ln(BK_{Li}Q^J_{+\infty}) \tag{30}$$

If the discussion described in the previous section is applicable to explain the characteristics of the experimentally measured potential, $\Delta\phi$, listed in Table 6, $\Delta\phi$ should be theoretically given by $\Delta\Phi$ represented by Eq. 31.

$$\Delta\Phi = (-\phi^L_0) - (-\phi^R_0) \tag{31}$$

$\Delta\Phi$ tuns into Eq. 32, and it is identical to the Nernst eq. Thus, the Nernst eq. in the physiological sense can be derived on the basis that the potential is generated by the spatial fixation of ions in this experimental system as well. But it must be proved experimentally or theoretically that the conditions Ⓐ and Ⓑ (see just below the Eq. 27) hold in order to validate the Eq. 32.

$$\Delta\Phi = \left(-\frac{kT}{e}\ln(BK_{Li}Q^L_{+\infty})\right) - \left(-\frac{kT}{e}\ln(BK_{Li}Q^R_{+\infty})\right) = -\frac{kT}{e}\ln\frac{Q^L_{+\infty}}{Q^R_{+\infty}} \tag{32}$$

ϕ^J_0 in Eq. 27 represents the surface potential of the lithium glass, but the potential data shown in Table 6 is not the surface potential but the potential across the lithium glass. Therefore, it is necessary to acquire the surface potential of the lithium glass by all means.

We need to measure the surface potential of the lithium glass immersed in the *LiCl* solution when the concentration of the bulk phase of *LiCl* is "$Q^J_{+\infty}$". Such an experimental

Preprints (www.preprints.org) | NOT PEER-REVIEWED | Posted: 16 May 2022 doi:10.20944/preprints202205.0200.v1

system should be equivalent to the system shown in Fig. 1 in a case where the $AgCl$ plate is replaced by the lithium glass and at the same time the KCl solution is replaced by the $LiCl$ solution. The authors have obtained such surface potentials before, as detailed in **Appendix A**, and the experimentally measured surface potential of lithium glass is abstracted in Table 7.

Table 7. Experimentally measured surface potentials of lithium glass and concentration of $LiCl$ solutions

$[LiCl]$ / M	10^{-5}	10^{-4}	10^{-3}	10^{-2}	10^{-1}	1
Surface potential / V	0.014	0.044	0.102	0.159	0.212	0.278

Secondly, the authors found that all the experimental data of the potential are sufficient for Eq. 27 as suggested by the computational results presented in Table 6. The theoretical curves obtained by calculating the LHS of Eq. 27 are represented in Fig. 9 by the solid lines and the corresponding data given in Table 8 are also shown in Fig. 9 by the symbol •". The data represented by □ in Fig. 9 were computed using Eq. 4 instead of the LHS of Eq. 27 on purpose. Their numerical values are also given in Table 8. The data computed using the RHS of Eq. 4 deviate widely from the constant as clearly shown in Fig. 9. Therefore, the constancy of Eq. 27 must have some unknown scientific meanings. Eq. 28 is only invalid when $[LiCl]_L = 10^{-5}$M. So, although not perfectly, Eq. 32 is basically experimentally validated. Therefore, what is described in this section is supporting evidence for the ion adsorption mechanism as a mechanism for generating membrane potential.

Table 8. Experimental and Computational data

Q^L_{Li} / M	10^{-5}	10^{-4}	10^{-3}	10^{-2}	10^{-1}	10^{0}
ϕ^L_0 / V	0.014	0.044	0.102	0.159	0.212	0.278
$\sinh(\beta\phi^L_0)/\sqrt{Q^L_{Li}}$ †1	113.112	107.671	113.038	110.302	98.069	112.132
$\sqrt{Q^L_{Li}}\sinh(\beta\phi_0)$ †2	0.001	0.011	0.113	1.103	9.807	112.132

†1 $\sinh(\beta\phi^L_0)/\sqrt{Q^L_{Li}}$ (LHS of Eq. 27) is almost constant.

†2 $\sqrt{Q^L_{Li}}\sinh(\beta\phi^L_0)$ (RHS of Eq. 4) is not constant at all.

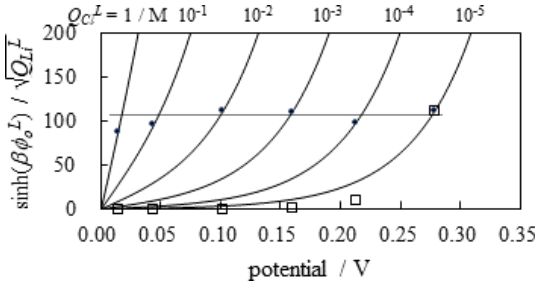

Figure 9. The theoretical computational curves of LHS of Eq. 27 are shown and the corresponding data shown in Table 6 is also shown by the symbol "•". "□" represents the computational values obtained by using Eq. 4. The dashed line represents Eq. 27.

According to the discussion so far made, the experimentally measured potential shown in Fig. 8 must be explicable by the adsorption mechanism. In other words, the theoretical potential $\Delta\Phi$ can be obtained using the surface potential shown in Table 7. Inserting the data from Table 7 into Eq. 33 yields the data presented in Fig. 10. Thus, Eq. 33 has clearly reproduced Fig. 8 as expected.

Preprints (www.preprints.org) | NOT PEER-REVIEWED | Posted: 16 May 2022 doi:10.20944/preprints202205.0200.v1

$$\begin{aligned} \Delta\Phi(xM) &= (-\phi_0^L(xM)) - (-\phi_0^R(XM)) \\ x &= 10^{-5}M \sim 1M,\ X \text{ is maintained constant } (= 10^{-5}M \sim 1M). \end{aligned} \tag{33}$$

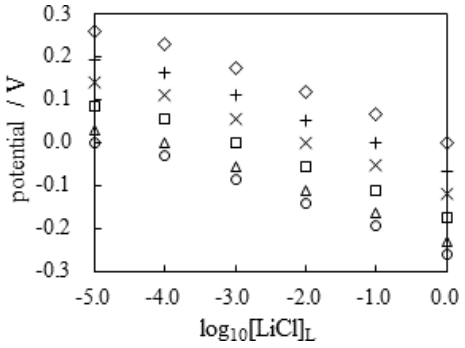

Figure 10. The data in Fig. 8 computed using Eq. 33 and the surface potential data shown in Table 5 ($[LiCl]_R$ = ◇: 10^{-5}M +: 10^{-4}M ×: 10^{-3}M □: 10^{-2}M △: 10^{-1}M ◯: 1M)

3.2. Potential of anionic hydrogel

Then, the potential profile of the hydrogel is studied experimentally and theoretically. Before starting the discussion, the notation table Table 9 is presented.

Table 9. Notations used in the section 3.2

ϕ_J^A	potential in J phase $J = s$(olution), g(el)
ϕ_0^A (= ϕ_g^A)	the gel surface potential (= potential gel inside)
$Q_{i+\infty}^A$	KCl the concentration of ion i in the solution bulk phase i where = H^+, K^+
$[i]_J^A$	concentration of i in J phase
K_i^A	association constant defined by $K_i = [COOi]_g/[-COO^-]_g[i]_g$
ρ_J^A	charge density in J phase
σ_0^A	interfacial charge density (per unit area) between the KCl solution and the anionic gel

Anionic hydrogels consisting of the chemicals listed in Table 10 were synthesized. The synthesized hydrogels were equilibrated in KCl solutions with concentrations ranging from 10^{-5}M to 1M. Next, the authors performed potential measurements of the hydrogels. The procedure for measuring the potentials is described as follows: Figure 11 shows the experimental setup with the coordinate system. The reference electrode $Ag/AgCl$ was inserted into the KCl solution phase and the indicator electrode $Ag/AgCl$ is inserted into the hydrogel. The measured potential is summarized in Table 11.

The potential profile of this system is theorized on the basis of the ion adsorption mechanism. The anionic hydrogel contains caroboxylic groups and they serve as ion adsorption sites. The reaction is represented by Eq. 34.

$$-COO^- + i^+ <=> -COOH \quad i = H^+, K^+ \tag{34}$$

Eq. 35 establishes where K_i^A is association constant.

$$K_i^A = \frac{[COOi]_g}{[-COO^-]_g[i]_g} \quad i = H^+, K^+ \tag{35}$$

Preprints (www.preprints.org) | NOT PEER-REVIEWED | Posted: 16 May 2022 doi:10.20944/preprints202205.0200.v1

Table 10. Chemical compositions of anionic hydrogel

chemicals	AAm[1]	AA[2]	TEMED[3]	MBA[4]	AP[5]	DI[6]
anionic gel / g	4.26	1.44	a few drops	0.077	0.044	50.0

[1] acrylamide
[2] allylamine hydrochlroride
[3] N,N,N′,N′tetramethylethylenediamine
[4] N,N methylenebisacrylamide
[5] ammonium persulfate
[6] deionized water

Table 11. Anionic hydrogel potential and its bathing KCl solution concentration

$[KCl]$ / M	10^{-5}	10^{-4}	10^{-3}	10^{-2}	10^{-1}	10^{0}
ϕ_g^A / V	-0.115	-0.081	-0.038	-0.013	-0.004	-0.000
$\sqrt{Q^A_{i+\infty}}\sinh(\beta\phi_g^A)$	-0.016	-0.024	-0.026	-0.026	-0.022	-0.020

Assuming that the potential of the anionic gel ϕ_g^A is uniform throughout the gel body, the expected potential profile should be represented by the dotted line in Fig. 11. For this system, $[K^+]_J$, $[H^+]_J$ and $[Cl^-]_J$ are given by Eq. 36 where $Q^A_{i+\infty}$ is the concentration of the ion "i" in the bulk phase.

$$\begin{aligned} [i]_J^A = \quad & Q^A_{i+\infty}\exp(-z_i 2\beta\phi_J^A) \\ i = \quad & K^+, H^+, Cl^-;\ J = \text{ s(olution phase), g(el phase)} \end{aligned} \tag{36}$$

Solution phase and gel phase charge densities are given by Eq. 37 where $[COO^-]_g$ exists only in the gel phase, hence, $[COO^-]_s \equiv 0$ in the KCl solution phase.

$$\rho_J^A = e([K^+]_J + [H^+]_J - [Cl^-]_J - [COO^-]_J), \quad [COO^-]_s = 0 \tag{37}$$

The P.-B. eq. given by Eq. 38 is derived and P.-B. eq. should suffice the conditions Eqs. 39 and 40.

$$\frac{d^2\phi_J^A}{dx^2} = -\frac{\rho_J^A}{\epsilon\epsilon_o} \tag{38}$$

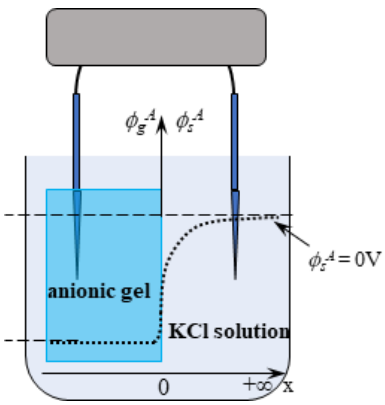

Figure 11. Experimental setup for measuring the potential of the hydrogel and its associated coordinate system

Preprints (www.preprints.org) | NOT PEER-REVIEWED | Posted: 16 May 2022 doi:10.20944/preprints202205.0200.v1

$$\phi_s^A \to 0 \ \ (x \to +\infty) \tag{39}$$

$$\frac{d\phi_J^A}{dx} \to 0 \ \ (x \to \pm\infty) \tag{40}$$

Since Eq. 41 holds in the almost whole range of KCl concentration in this experiment, Eq. 42 is derived.

$$[K^+]_J >> [H^+]_J \tag{41}$$

$$Q_{H+\infty}^A + Q_{K+\infty}^A \sim Q_{K+\infty}^A \tag{42}$$

Therefore, Eq. 38 turns out to be Eq. 43 where $Q_{Cl+\infty}^A$ is the bulk phase concentration of Cl^-.

$$\frac{d^2\phi_s^A}{dx^2} = -\frac{e}{\epsilon\epsilon_o}\left(Q_{K+\infty}^A \exp(-2\beta\phi_s^A) - Q_{Cl+\infty}^A \exp(+2\beta\phi_s^A)\right) \tag{43}$$

Due to the electroneutrality in the bulk phase of the solution, Eq. 44 is derived and it transforms Eq. 43 into Eq. 45.

$$Q_{K+\infty}^A = Q_{Cl+\infty}^A \equiv Q_{+\infty}^A \tag{44}$$

$$\frac{d^2\phi_s^A}{dx^2} = -\frac{eQ_{+\infty}^A}{\epsilon\epsilon_o}\left(\exp(-2\beta\phi_s^A) - \exp(+2\beta\phi_s^A)\right) \tag{45}$$

The authors have hypothesized that the potential in the gel phase represented by ϕ_g^A is constant everywhere in the gel body, including at its surface as described previously. Therefore, the charge density σ_0^A at the interface between the solution and the gel is derived following the same procedure described in the section 3.1 and is Eq. 46.

$$\sigma_0^A = -2\sqrt{2\epsilon\epsilon_o Q_{+\infty}^A kT}\sinh(\beta\phi_0^A) = -2\sqrt{2\epsilon\epsilon_o Q_{+\infty}^A kT}\sinh(\beta\phi_g^A) \tag{46}$$

Now, again the same (or similar) equation to Eqs. 4 or 27 has appeared. The authors were intrigued to see if Eq. 47 derived from Eq. 46 could hold. Figure 12 shows the theoretical LHS curve of Eq. 47. Figure 12 shows the theoretical LHS curve of equation 47 as a function of ϕ_0^A and at the same time their values computed using the experimental data of $Q_{+\infty}^A$ and ϕ_0^A ($= \phi_g^A$) listed in Table 11 are also shown by "•".

$$\sqrt{Q_{+\infty}^A}\sinh(\beta\phi_0^A) = \sqrt{Q_{+\infty}^A}\sinh(\beta\phi_g^A) \sim const. \tag{47}$$

The LHS values of Eq. 47 computed using the experimental data of $Q_{+\infty}^A$ and ϕ_g^A appear to be held basically constant. Hence, the last term of Eq. 47 is "const."

Eq. 47 cannot be transformed into a Nernst eq. as described in section 3.1, since the Eq. 48 approximation is invalid in light of the experimentally measured ϕ_g^A potential in

Preprints (www.preprints.org) | NOT PEER-REVIEWED | Posted: 16 May 2022 doi:10.20944/preprints202205.0200.v1

Table 11. Furthermore, the ϕ_g^A vs. $\log_{10}[KCl]$" profile represented by the "•" symbol in Fig. 13 is outside the Nernst eq. from the start. However, there seems to be a constraint on the characteristics of the potential as given by the Nernst eq. 47.

$$\sinh(\beta\phi_g^A) \sim \exp(-\beta\phi_g^A) \tag{48}$$

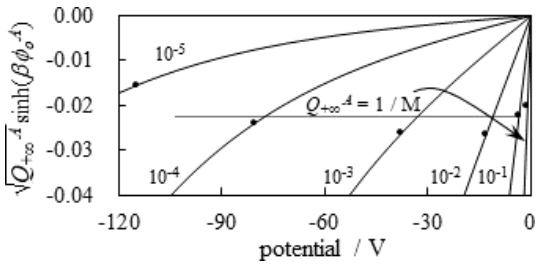

Figure 12. The theoretical computational curves of Eq. 47 LHS and the corresponding data shown in Table 11 indicated by the symbol "•". The dashed line represents Eq. 47.

Now, we have examined Eq. 47 from a computational perspective. Figure 12 indicates that Eq. 47 can be approximately given by the equation 49. Solving Eq. 49 with respect to ϕ_g^A yields the data shown in Fig. 13 by the symbol "□". The experimental and computed ϕ_g^A show good agreement with each other.

$$\sqrt{Q_{+\infty}^A}\sinh(\beta\phi_g^A) \sim -0.022 \tag{49}$$

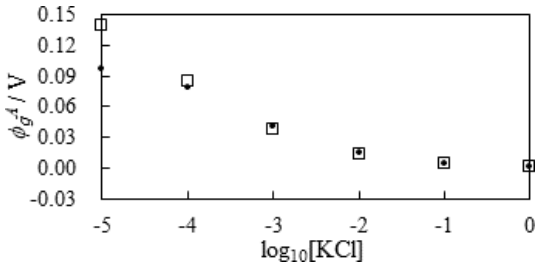

Figure 13. ϕ_g^A vs. $\log_{10}[KCl]$ •: Experimental □: Computationally obtained from Eq. 49

3.3. Potential of cationic hydrogel

The same analysis was performed with the cationic hydrogel. Before showing the results, the notation table Table 12 is given.

Table 12. Notations used in the section 3.3

ϕ_J^C	potential in J phase $J = s$(olution), g(el)
ϕ_0^C (= ϕ_g^C)	the gel surface potential (= potential gel inside)
$Q_{i+\infty}^C$	KCl the concentration of ion Cl^- in the solution bulk phase
$[i]_J^C$	concentration of i in j phase
$K_{C]}^C$	association constant defined by $K_{Cl} = [NH_3Cl]_g/[-NH_3^+]_g[Cl^-]_g$
ρ_J^C	charge density in j phase
σ_0^C	interfacial charge density between the KCl solution and the anionic gel

Cationic hydrogels composed of the chemicals listed in Table 13 were synthesised. The synthesised hydrogels were equilibrated in KCl solutions ranging from 10^{-5}M to 1M. Next,

Preprints (www.preprints.org) | NOT PEER-REVIEWED | Posted: 16 May 2022 doi:10.20944/preprints202205.0200.v1

the authors measured the potentials of the hydrogels using the same method as that used to measure the potential of the anionic gels. The measured potentials are summarized in Table 14.

Table 13. Chemical compositions of cationic hydrogel

chemicals	AAm[1]	Al[2]	TEMED[3]	MBA[4]	AP[5]	DI[6]
cationic gel / g	4.26	1.86	a few drops	0.077	0.044	50.0

[1] acrylamide
[2] allylamine hydrochlroride
[3] N,N,N′,N′tetramethylethylenediamine
[4] N,N methylenebisacrylamide
[5] ammonium persulfate
[6] deionized water

Table 14. Cationic hydrogel potential and its bathing KCl solution concentration

$[KCl]$ / M	10^{-5}	10^{-4}	10^{-3}	10^{-2}	10^{-1}	10^{0}
ϕ_g^C / V	0.099	0.073	0.039	0.017	0.005	0.001
$\sqrt{Q_{Cl}^C}\sinh(\beta\phi_g^C)$	0.011	0.020	0.027	0.035	0.028	0.020

The potential profile of this system is theorized on the basis of the ion adsorption mechanism. The anionic hydrogel contains amino groups that serve as adsorption sites for the ions. The reaction is represented by the Eq. 50.

$$-NH_3^+ + Cl^- <=> -NH_3^+Cl^- \tag{50}$$

Eq. 51 establishes where K_{Cl}^C is an association constant.

$$K_{Cl}^C = \frac{[NH_3^+Cl^-]_g}{[-NH_3^+]_g[Cl^-]_g} \tag{51}$$

Assuming that the potential of the cationic gel ϕ_g^C is uniform throughout the gel body. $[K^+]_k$, $[H^+]_k$ and $[Cl^-]_k$ are given by Eq. 52.

$$\begin{aligned} [i]_J^C = \quad & Q_{J+\infty}^C \exp(-z_i 2\beta\phi_J^C) \\ i: \quad & K^+, H^+, Cl^- \quad J: \text{ s(olution phase), g(el phase)} \end{aligned} \tag{52}$$

The charge densities in the solution and gel phases are given by equation 53 where $[NH_3^+]_g$ exists only in the gel phase.

$$\rho_J^C = e([K^+]_J + [H^+]_J - [Cl^-]_J + [-NH_3^+]_J), \quad [-NH_3^+]_s = 0 \tag{53}$$

The P.-B. eq. given by Eqs. 54 is derived and the P.-B. eq. should suffices the conditions Eqs. 55 and 56.

$$\frac{d^2\phi_J^C}{dx^2} = -\frac{\rho_J^C}{\epsilon\epsilon_o} \tag{54}$$

Preprints (www.preprints.org) | NOT PEER-REVIEWED | Posted: 16 May 2022 doi:10.20944/preprints202205.0200.v1

$$\phi_s^C \to 0 \ \ (x \to +\infty) \tag{55}$$

$$\frac{d\phi_J^C}{dx} \to 0 \ \ (x \to \pm\infty) \tag{56}$$

Since Eq. 57 is valid over almost the entire concentration range of KCl in this experiment, Eq. 58 is derived, where $Q_{i+\infty}^C$ is the ion "i" concentration in the bulk phase.

$$[K^+]_J >> [H^+]_J \tag{57}$$

$$Q_{H+\infty}^C + Q_{K+\infty}^C \sim Q_{K+\infty}^C \tag{58}$$

Therefore, Eq. 54 turns into Eq. 59.

$$\frac{d^2\phi_s^C}{dx^2} = -\frac{e}{\epsilon\epsilon_o}\left(Q_{K+\infty}^C \exp(-2\beta\phi_s^C) - Q_{Cl+\infty}^C \exp(+2\beta\phi_s^C)\right) \tag{59}$$

Due to the electroneutrality in the bulk phase of the solution phase, Eq. 60 is derived and it transforms Eq. 59 into Eq. 61.

$$Q_{K+\infty}^A = Q_{Cl+\infty}^A \equiv Q_{+\infty}^A \tag{60}$$

$$\frac{d^2\phi_s^C}{dx^2} = -\frac{eQ_{+\infty}^C}{\epsilon\epsilon_o}\left(\exp(-2\beta\phi_s^C) - \exp(+2\beta\phi_s^C)\right) \tag{61}$$

The authors have assumed that the potential in the gel phase represented by ϕ_g^C is constant throughout the gel body including its surface. Therefore, the charge density σ_0^C at the interface between the solution and the gel is derived following the same procedure described in section 3.1 and is Eq. 62.

$$\sigma_0^C = -2\sqrt{2\epsilon\epsilon_o Q_{+\infty}^C kT}\sinh(\beta\phi_0^C) = -2\sqrt{2\epsilon\epsilon_o Q_{+\infty}^C kT}\sinh(\beta\phi_g^C) \tag{62}$$

Once again, the same (or similar) equation to Eqs. 4 or 27 arose. Eq. 63 is derived from Eq. 62 by guess in the course of our discussion so far made. The theoretical curves of the LHS of Eq. 62 are shown in Fig 14. The numerical values of the leftmost term of Eq. 63 computed using the experimental data of $Q_{+\infty}^C$ and ϕ_s^C are summarized in Table 14 and are shown in Fig. 14 as well as by "•".

$$\sqrt{Q_{+\infty}^C}\sinh(\beta\phi_0^C) \sim \sqrt{Q_{+\infty}^C}\sinh(\beta\phi_g^C) \sim const. \tag{63}$$

Although not perfect, the numerical values of the LHS of Eq. 63 are in a relatively narrow range independently of $Q_{+\infty}^C$. Hence, we concluded that Eq. 63 is relatively well established.

Similar to what is described in the previous section, ϕ_g^C does not obey the Nernst eq. (see the potential data represented by the symbol "•" in Fig. 15). However, there seems to be a constraint on the characteristics of the potential represented by Eq. 46. We then

Preprints (www.preprints.org) | NOT PEER-REVIEWED | Posted: 16 May 2022 doi:10.20944/preprints202205.0200.v1

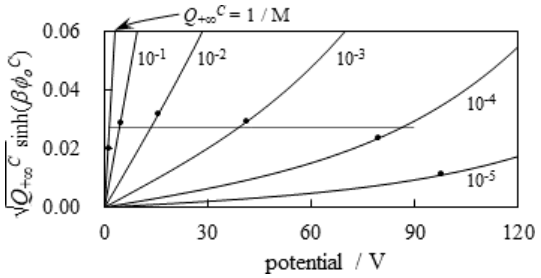

Figure 14. The theoretical computational curves of LHS of Eq. 47 is shown and the corresponding data shown in Table 14 is also shown by the symbol "•". The dashed line represents Eq. 62.

examined Eq. 63 computationally. Figure 14 indicates that Eq. 63 can be approximately given by Eq. 64. Solving Eq. 64 with respect to ϕ_g^C yields the data shown in Fig. 15 by the symbol "□". The experimental and computed ϕ_g^C show good agreement with each other.

$$\sqrt{Q_{+\infty}^C}\sinh(\beta\phi_g^C) \sim +0.026 \tag{64}$$

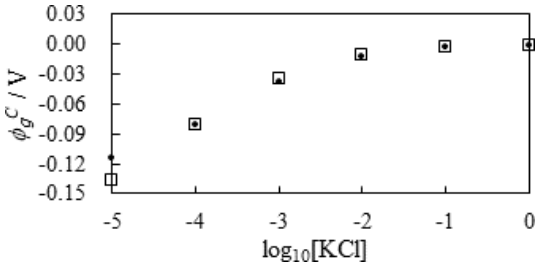

Figure 15. ϕ_g^C vs. $\log_{10}[KCl]$ •: Experimental □: Computationally obtained from Eq. 64

4. Key equation and what it suggests

The authors noted from the studies described above that the theoretical basis of membrane potential lies in the Eq. 65, which even leads to the formula identical to the Nernst eq. Eq. 65 is derived using the Boltzmann distribution, the law of mass action and the Langmuir isotherm. There is therefore nothing contradictory with thermodynamics and physical chemistry. Namely, Eqs. 4, 27, 47 and 62 are heavily related to Eq. 65. More precisely, the origin of these equations except for Eq. 26 are Eqs. 2, 20 and 46 and these equations suggest that the charge density of the surface (or interface) is held constant regardless of the ion concentration of the bath solution. Why is the charge density of the surface (or interface) constant?

$$Q^{\pm 1/2}\sinh(\beta\phi) \sim const. \tag{65}$$

It is perhaps not so hasty and unwise to say that there is something in common in the four experimental systems described above. All experimental systems deal with electrolytic aqueous solution systems. Thus, all systems have a large number of water molecules. It is known that water molecules are adsorbed on the surfaces of materials. Their adsorption strength is sometimes extremely high, and it is practically impossible to remove the water molecules from the surface of the material [1,8]. Therefore, it is highly doubtful that such a layer of water molecules covering the surface of the material has no influence on the adsorption of ions and/or the potential generation mechanism.

 doi:10.20944/preprints202205.0200.v1

Pollack's work is quite suggestive. He studied the bound water layer formed on the surfaces of materials. He found that the surface of a hydrophilic material in contact with water is inevitably covered with water molecules, called structured water, and that the structured water layer tends to expel small substances. He calls this layer the "exclusion zone, EZ". [9–14]. EZ has unique electrical characteristics. According to Pollack, EZ itself carries a non-zero potential. Thus, the formation of the structured water has a significant influence even on the potential characteristics. Even if the characteristics of the material, such as its surface structure, are different from one material to another, if the surface is covered with a layer of structured water, regardless of the species of the material, the ion adsorption sites on the surface are inevitably subject to the strong influence of the same water. Ion adsorption could occur through structured water layers covering both the ion adsorption sites and the ions. If this is the case, it is not so anomalous that a certain potential characteristic in the electrolyte solution system is governed by a single rather simple law such as Eq. 65. Eq. 26 does not represents the surface charge density but is constant. Therefore, Eq. 26 must also have some profound meaning involving the water molecule characteristics.

5. Conclusion

The authors found that membrane potentials appear to be governed by a single equation Eq. 65 regardless of the systems in question, though we have been unable to justify this speculation theoretically yet. It is in some cases even possible to derive the potential formula identical to Nernst eq. by using Eq. 65. Our idea is based on the ion adsorption mechanism and the ion adsorption mechanism is fully in line with the thermodynamics and physical chemistry.

We suggested the works on water characteristics which are especially well featured by the Pollack's work as one of the significant clues for the elucidating the meaning of Eq. 65. Water is common for all the systems employed for the membrane potential studies. The characteristics of such a common substance, water, may play a central role of membrane potential characteristics governed by Eq. 65. Further study is awaited for elucidating the membrane potential generation mechanism.

Declaration of COI: The author states that there is no conflict of interest.

1. Gilbert N. Ling. *A Revolution in the Physiology of the Living Cell*; Krieger Pub Co, Malabar, Florida, 1992.
2. Gilbert Ling. *Debunking the alleged resurrection of the sodium pump hypothesis.* Physiol. Chem. Phys. 1997, 29, 123—-198.
3. Gilbert N. Ling. *Life at the Cell and Below-Cell Level: The Hidden History of a Fundamental Revolution in Biology*; Pacific Press, New York, 2001.
4. H. Tamagawa. *Mathematical expression of membrane potential based on Ling's adsorption theory is approximately the same as the Goldman–Hodgkin–Katz equation*. J. Biol. Phys. 2018, 45, 13–30.
5. H. Tamagawa, K. Ikeda. *Another interpretation of Goldman-Hodgkin-Katz equation based on the Ling's adsorption theory*. Eur. Biophys. J. 2018, 47, 869–879.
6. Khalid R. Temsamani, K. Lu Cheng. *Studies of chloride adsorption on the Ag/AgCl electrode*. Sensors and Actuators B 2001, 76, 551–555.
7. Gordon M. Barrow. *Physical Chemistry*; McGraw-Hill Inc.: New York, US, 1984.
8. Jacob N. Israelachvili. *Intermolecular and Surface Forces: With Applications to Colloidal and Biological Systems*; Academic Pres, MA, USA, 2015.
9. J. Zheng J, G. H. Pollack. *Solute Exclusion and Potential Distribution Near Hydrophilic Surfaces. In: G.H. Pollack, I. L. Cameron, D. N. Wheatley (eds) Water and the Cell*; Springer, Dordrecht, 2006.
10. J. Zheng, W. Chin, E. Khijniak, E. Khijniak, G. H. Pollack. *Surfaces and interfacial water: Evidence that hydrophilic surfaces have long-range impact.* Advances in Colloid and Interface Science 2006, 127, 19–27.
11. J. Zheng, A. Wexler, G. H. Pollack. *Effect of buffers on aqueous solute-exclusion zones around ion-exchange resins.* Journal of Colloid and Interface Science 2009, 332, 511—-514.

12. G. H. Pollack. *The Fourth Phase of Water: Beyond Solid, Liquid, and Vapor*. Edgescience 2013, 16, 14.
13. Gerald H. Pollack. *The Fourth Phase of Water: Beyond Solid, Liquid, and Vapor*; Ebner & Sons, Seattle, USA, 2014.
14. Daniel C. Elton, Peter D. Spencer, James D. Riches, Elizabeth D. Williams. *Exclusion Zone Phenomena in Water—A Critical Review of Experimental Findings and Theories*. Int. J. Mol. Sci. 2020, 21, 5041. doi:10.3390/ijms21145041.

Appendix A

Unlike the *AgCl* plate, the surface potential of lithium glass immersed in a *LiCl* solution is not easily measured. In various experiments, the authors noticed that the potential across the lithium glass is indifferent to the concentration of *KCl* in contact with the lithium glass surface. This phenomenon is briefly explained below.

The authors measured the potential generated across the lithium glass between a *LiCl* solution and a *KCl* solution. The potential measurement was carried out using a setup virtually identical to that shown in Fig. 5 where the *AgCl* plate was replaced by the lithium glass and the right-hand phase solution was 10^{-4}M *KCl*, while the left-hand phase solution was the *LiCl* solution whose concentration varied from 10^{-5}M to 1M. The authors performed the same potential measurements again but the right-hand phase solution was replaced by a 10^{-2}M *KCl* solution and the measured potentials were almost the same as those where the *KCl* concentration was 10^{-4}M as shown in Fig. A.1.

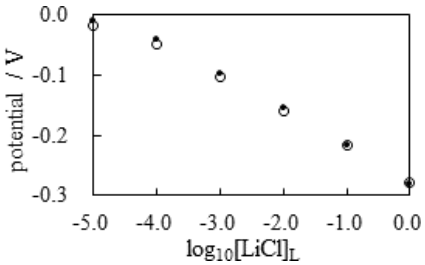

Figure A.1. Experimentally measured potential across the lithium glass intervening a *LiCl* solution and a *KCl* solution The Left phase *LiCl* concentration is varied from 10^{-5}M through 1M while the Right phase *KCl* concentration is maintained constant, ◯: 10^{-4} or •: 10^{-2}M

The authors interpreted these results as follows: Figure A.2 represents the system consisting of a lithium glass intervening between a *LiCl* solution and a *KCl* solution. Since the potential of the lithium glass surface is indifferent to the concentration of the *KCl* solution in contact with the straight surface of the lithium glass, the potential in the straight phase is assumed to be constant as shown in Fig. A.2. Therefore, the potentials measured across the lithium glass virtually correspond to the "ϕ_0^L" surface potential shown in Fig. A.2. Hence, the potential data shown in Fig. A.1 is shown in Table 7 which can be interpreted as the surface potentials of the lithium glass in contact with the *LiCl* solution.

 doi:10.20944/preprints202205.0200.v1

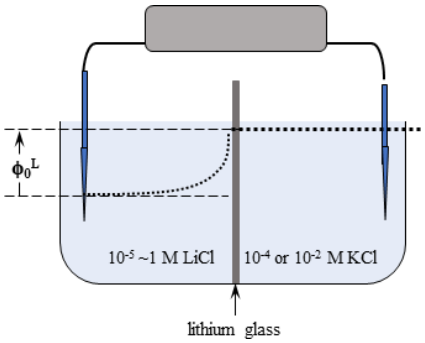

Figure A.2. Experimental setup for measuring the potential across the lithium glass intervening a *LiCl* solution and a *KCl* solution The Left phase *LiCl* concentration is varied while the Right phase *KCl* concentration is maintained constant (10^{-4}M or 10^{-2}M). The dotted line represents the expected potential curve.